Natural multiscale channeled salt resistant solar evaporator for efficient and long-term water desalination

Li, Yongzheng; Wang, Xiaodi; Wu, Ruijie; Qin, Jinli; Fu, Yingjuan; Qin, Menghua; Zhang, Yongchao; Xu, Chunlin

Published in:
Industrial Crops and Products

DOI:
10.1016/j.indcrop.2023.117649

Published: 15/12/2023

Document Version
Final published version

Document License
CC BY

Industrial Crops & Products 206 (2023) 117649

Contents lists available at ScienceDirect

Industrial Crops & Products

journal homepage: www.elsevier.com/locate/indcrop

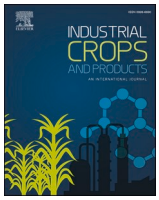

Natural multiscale channeled salt resistant solar evaporator for efficient and long-term water desalination

Yongzheng Li [a], Xiaodi Wang [b], Ruijie Wu [c], Jinli Qin [d], Yingjuan Fu [a], Menghua Qin [b], Yongchao Zhang [a,*], Chunlin Xu [c,*]

[a] State Key Laboratory of Biobased Material and Green Papermaking, Qilu University of Technology, Shandong Academy of Sciences, Jinan 250353, Shandong, China
[b] Organic Chemistry Laboratory, Taishan University, Taian 271021, China
[c] Laboratory of Natural Materials Technology, Åbo Akademi University, Turku FI-20500, Finland
[d] Materials Science Institute, Sun Yat-Sen University, Guangzhou 510275, China

ARTICLE INFO

Keywords:
Solar steam evaporation
High efficiency
Tree root
Multiscale channels
Graphene oxide
Anti-salt-accumulation

ABSTRACT

Solar steam evaporation exhibits great potential in solving the global shortage of freshwater resources. However, salt accumulation at the top photothermal conversion surface has severely limited the desalination efficiency and stability of solar desalination systems. Herein, we demonstrated a nature-inspired salt resistant bilayered evaporator by using a slight delignificated tree root as bottom substrate and decorated graphene oxide layer as the top absorber surface. The naturally design of tree root inherently exists multilevel vertical channels interconnected porous microstructures. This distinctive structure of tree root allows ultra-high-speed water transport capability and rapid multi-directional salt exchange, enabling it to possess anti-salt-accumulation properties for solar steam generation. This designed tree root-based evaporator effectively prevented salt accumulation while maintaining a fast and stable evaporation rate, which exhibited an evaporation rate of 1.60 kg m^{-2} h^{-1} with excellent long-term stability in a high-salinity brine (21 wt%) under 1 sun irradiation. Taking the unparalleled advantages, our designed tree root-based evaporator obtained by a facile fabrication method represents a high-efficacy and stable fresh water production platform for practical applications in water purification.

1. Introduction

Freshwater is closely related to the survival of all life on the earth, and is one of the most essential resources required for human sustainable development (Kumar et al., 2021; Kummu et al., 2016). According to the report from United Nations (UN), 2.7 billion people will suffer from severe water scarcity problems by 2025, which is an urgent challenge faced by humanity (Kumar et al., 2021; Mekonnen and Hoekstra, 2016; Rana et al., 2021). Seawater is an inexpensive widely available resource on our planet, covering nearly 71% of the Earth' surface (He et al., 2021). Free solar energy is deemed as a representative of the clean and renewable energy sources (Al-Douri and Fayadh, 2016). Taking the advantage of the abundant resources, solar desalination technology has been proposed as a promising strategy to address the global freshwater scarcity (Chen et al., 2019; Djellabi et al., 2022; Zang et al., 2021). The typical interfacial solar steam evaporator is composed of a light absorber layer for generating steam by photothermal conversion and a bottom supporting substrate for transferring and supplying the water lost from top layer (Cao et al., 2021; Zang et al., 2021).

In order to achieve efficient photothermal convention, two key design principles are required: (a) adequate light absorption by a black layer over a broad wavelength range; (b) efficient heat management to reduce the heat diffusion from top light absorber layer. Various photothermal conversion materials, including carbon materials (Weixin et al., 2021), plasmas (metallic nanostructures) (Fujun et al., 2018) and composite polymer materials (Jingjing et al., 2020), have been widely explored for solar steam evaporation. Among them, graphene has been considered as a revolutionary material due to its outstanding light absorption capacity, thermal management and chemical stability (Dengyu et al., 2020). To enhance the photothermal conversion efficiency, great efforts have been devoted to design 3D structured graphene, such as 3D graphene-based foam or aerogel (Duan et al., 2021; Li et al., 2023; Zheng et al., 2023), and modify with additional functional polymers, such as metal-organic framework (Han et al., 2021), polybenzoxazine resin and cellulose fibers (Peng et al., 2021; Storer et al., 2020). These strategies involved either costly raw materials or complex fabrication processes,

* Corresponding authors.
E-mail addresses: yongchaoaaaa@163.com (Y. Zhang), cxu@abo.fi (C. Xu).

https://doi.org/10.1016/j.indcrop.2023.117649
Received 5 August 2023; Received in revised form 14 October 2023; Accepted 16 October 2023
Available online 17 October 2023

which limited their practical applications. Furthermore, salt accumulation related issues, occurred during the solar desalination process, remain challenge to overcome (Bian et al., 2021; Chen et al., 2019). The accumulated salt crystals on the absorber interface could block sunlight and clog water transport channels, resulting in the reduction of evaporation efficiency or even interrupt the desalination (He et al., 2019; Kuang et al., 2019). Therefore, achieving a practical solar evaporator with low-cost, facile production, high-efficiency and long-term stability, is highly desired.

The selection and design of the bottom supporting materials of solar evaporators can play a pivotal role in addressing salt-accumulation related issues, where the critical considerations can be summarized as follows: (a) high water transfer capability from bulk water to the top evaporator surface, continuously supplying the evaporative water loss; (b) efficient salt exchange between the concentrated saline with the bulk solution, preventing salt accumulation on the absorber interface; (c) low thermal conductivity, reducing the thermal diffusion from the upper surface (Cao et al., 2021; He et al., 2019; Kuang et al., 2019). Considering the biodegradability, wide availability and renewability, natural wood has been used as an promising substrate for fabricating solar evaporators (Li et al., 2018; Xue et al., 2017; Zhu et al., 2018). The inherent mesoporous microstructures and physicochemical properties endow the effective water transfer ability and low thermal conductivity to natural wood (Cao et al., 2021; Jia et al., 2017; Li et al., 2018). However, the natural wood structures without additional processing are still insurmountable to achieve the salt resistance of solar desalination devices. For example, wood based solar evaporators with salt-rejecting property was prepared by drilling millimeter-sized channels (Kuang et al., 2019; Sharshir et al., 2022). Many recent reported wood-based solar evaporators showed mediocre performance, one of the main challenges needed to overcome is the inability to combine high thermal conversion efficiency with salt resistance (Ma et al., 2020; Xue et al., 2017). A feasible solar vapor generation system for water purification should possess continuous water transportation, efficient energy capture, and solar-thermal conversion to ensure the highly efficient water purification capability.

Herein, we designed an anti-salt-accumulation solar evaporator by combining natural tree-root based supporting substrate and graphene oxide decorated interface, simultaneously achieving high efficiency and long-term operational stability. Compared to the wood trunks with vertically aligned microchannels along the growth direction, the tree roots with naturally hierarchical design of show multilevel vertical channels (including micrometer and millimeter-scale) and low curved channel millimeter-sized large channels (Fig. 1). During continuous solar desalination process, the accumulated brine concentration in the millimeter-sized channels was lower than that of narrow channels, causing the forced salt exchange between the multi-level channels driven by concentration difference. The multidirectional salt exchange between nearby channels prevented narrow channels from being blocked by generated salt crystals, eventually the concentrated salt was dissolved back into the bottom bulk water. As a proof-of-concept, our graphene oxide decorated tree root rendered an evaporation rate of 1.60 kg m^{-2} h^{-1}, and exhibited no salt-accumulation over 72 h continuous solar evaporation. The facile fabrication of bilayered solar desalination device using such low-cost and scalable raw materials demonstrates the promising potential for large-scale practical applications.

2. Materials and methods

In this work, the wood used was elm wood root, which was obtained from north of China. Graphene oxide (GO) dispersion was purchased from Xianfeng Nano Material Technology Co., Ltd. All the chemicals were analytical grade.

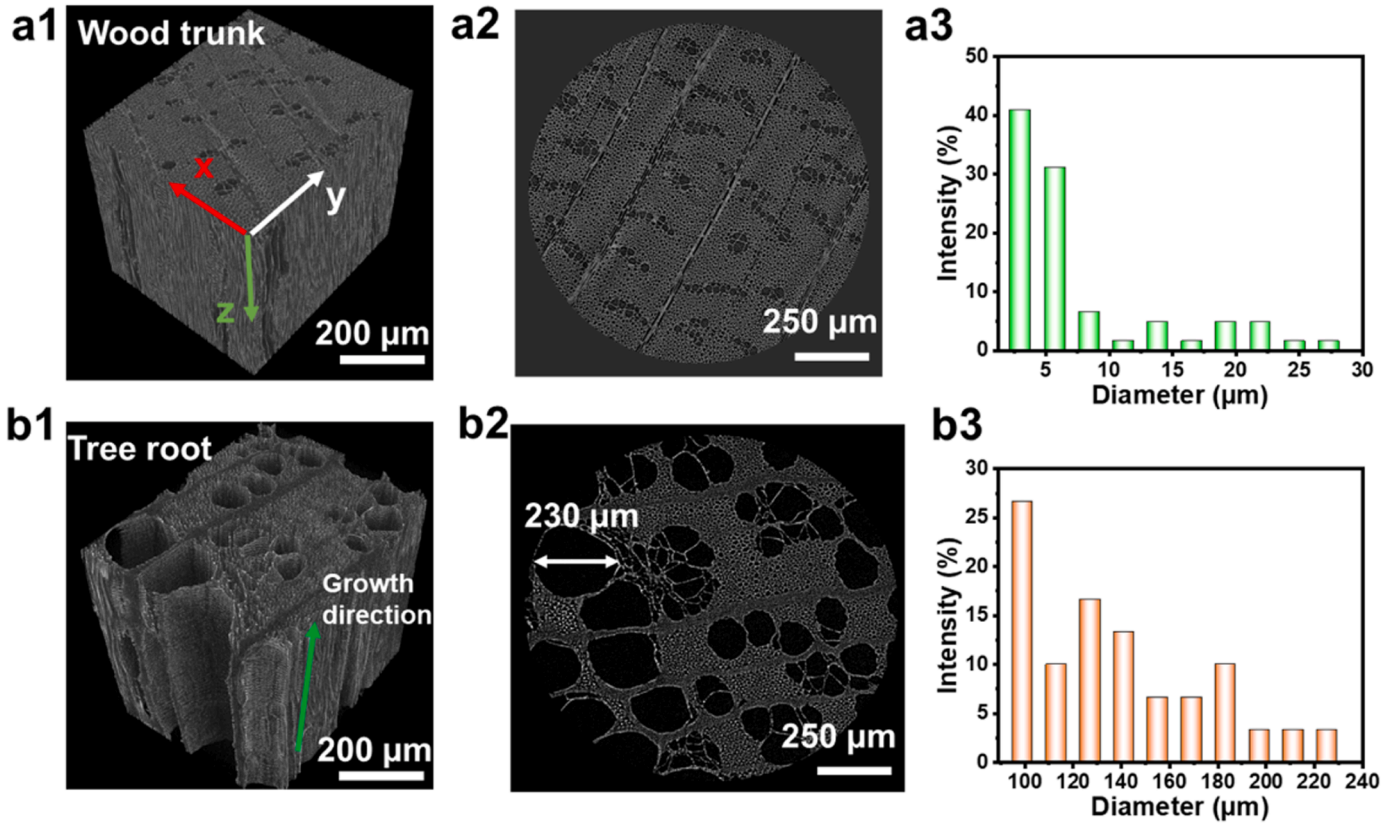

Fig. 1. 3D and 2D micro-CT tomographic images of the microchannels along the growth direction in wood trunk (a1 and a2) and tree root (b1 and b2). Size distribution of channel diameter in wood trunk (a3) and tree root (b3).

2.1. Preparation of GO decorated tree-root based solar evaporator (DRGO)

Firstly, 3 mm thick natural elm wood roots were cut along the channel direction. Then, elm wood root chips were impregnated in the 12 wt% NaOH solution and kept boiling and stirring at 100 °C for 3 h. After washing with hot distilled water, the top surface of the delignificated elm wood roots were covered with graphene oxide solution (10 mg/mL), forming an uniform coating layer. After oven drying, the graphene oxide decorated tree-root based solar evaporator was obtained. The stability of graphene oxide on the surface of the solar evaporator was evaluated by being immersed in various concentration of acid and alkaline solution.

2.2. Solar evaporation experiments

Solar desalination for interfacial experiment was performed by making homemade evaporation system. Xenon lamp light source was applied to simulate sunlight by adjusting power with light power meter (NP200–2A, Beijing, China). DRGO evaporator was placed at area of glass dish and floated in saline solution. The weight of glass dish was recorded by electronic scale with an accuracy 0.0001 g. Reduction in overall mass of water at dark environment and solar illumination were noted in real-time. In the meantime, the surface temperature of seawater and DRGO evaporator were recorded with infrared thermal imaging camera for calculating the solar transformation efficiency. The evaporation efficiency was calculated according to previous researches (Chen et al., 2019; 2017). The temperature was maintained at 20 ± 0.5 °C throughout the experiment.

2.3. Material characterization

The sample internal microstructure was analyzed by SEM (Hitachi Regulus8220, Japan). The samples were cut into a square of volume 8 mm^3 (2 ×2 ×2 mm) to observe by micro-computed tomography (micro-CT, Bruker SkyScan2211 Germany). The wettability of samples was presented by contact angle (CA, OCA50, Germany). Infrared photos were shot by using IR camera (FOTRIC, China), and real-time temperature change was monitored. The diffusive reflection spectra were recorded by the ultraviolet-visible-near infrared spectrophotometer (UV-Vis-NIR, Agilent Cary 5000, America). The thermal conductivity was tested referencing to international standards (ISO 22007–2) by hotdisk (TPS2500s, Sweden).

3. Results and discussion

3.1. Design and microstructure characterization of DRGO

Fig. 2a illustrated the facile process for fabricating DRGO. Two simple modifications were conducted to improve the evaporation performance. Firstly, the hydrophobic lignin was partly removed from raw tree root by treatment with 12% sodium hydroxide solution at 90 ℃, converting tree root into a super hydrophilic material, thus increasing the hydraulic conductivity of the supporting substrate of the solar

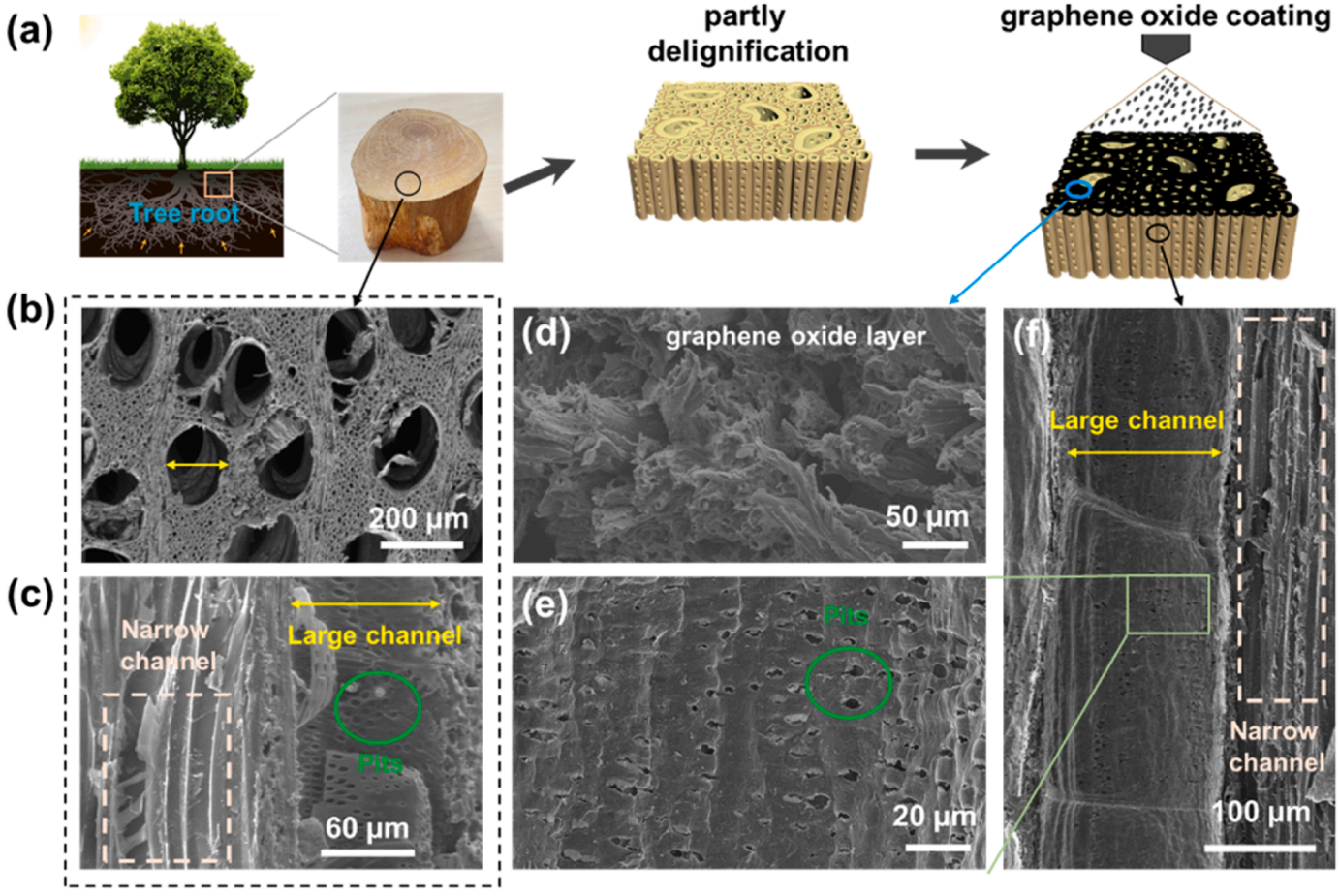

Fig. 2. (a) Schematic illustration of DRGO with multilevel channel structured tree root as bottom supply substrate and coated graphene oxide layer as top light absorber. (b) Top view SEM image of tree root shows large channels surrounded by numerous narrow channels along the tree growth direction. Longitudinal sectional view SEM image of tree root (c) and the fabricated evaporator (f) shows vertically aligned multilevel channels. (d) Top view SEM image of the fabricated evaporator shows uneven surface. (e) SEM image of the cell wall of one large channel shows numerous pits.

evaporator. Secondly, graphene oxide was loaded on the top surface of the delignificated tree root, forming a light absorption interface. Using the bilayer designed solar desalination device, the bottom hydrophilic tree root substrate continuously transported saline upward to the upper evaporation layer by capillary force, while the top graphene oxide decorated interface rapidly conducted photothermal conversion to generate steam.

The three-dimensional (3D) microstructure of tree root was illustrated by micro-CT and scanning electron microscopy (SEM). The low tortuosity multi-level vertically channels run through the entire cross section along the growth direction, providing multitudinous transport pathways (Fig. 1a1 and Fig. S1). Compared with the channel-array structure of wood trunk, tree root exhibited natural larger vertically aligned channels surrounded by narrow channels (Fig. 1a2 and b2). Approximately 71% of narrow channels in tree root were less than 30 μm in diameter, and 13% of lager channels ranged between 100 and 250 μm in diameter, while the vertically aligned channels in wood trunk below 30 μm in diameter (Fig. 1a3 and b3). The large channels played the same important role as artificial drilled holes of wood in terms of salt resistance during continuously solar evaporation process (Kuang et al., 2019). The salt concentration of the vertically aligned multi-level channels continuously increased with the generation of steam on the evaporation layer. The corresponding hydraulic conductivity of large channels was higher than that of narrow channels, leading to the salt concentrations remained in large channels are progressively lower than those in the narrow channels. Specifically, the multi-level tree root channels were interconnected by the numerous holes, named pits observed on the channel wall (Fig. 2c and e), offering connected routes for multidirectional salt exchange between neighboring channels under the generated salt gradient. The concentrated saline in narrow channels can be efficient diluted into the large channels, and further dissolved back into the bottom bulk water. Note that after delignification and graphene oxide decoration of tree root, the multi-level vertically aligned channels and interconnected pits were well remained (Fig. 2c, e and f), demonstrating the modification processes did not cause serious damage or blockage to the tree root inside microstructures. Remarkably, the graphene oxide decorated absorber layer based on the delignificated tree root showed abundant protrusion microstructures (Fig. 2d), significantly increasing the surface area for broader sunlight absorption. All these unique microstructures were the critical factors to achieve excellent salt resistance property and high-efficiency photothermal conversion during the solar desalination process.

XPS was used to examine the surface elemental composition of delignificated tree root (DR) and delignificated tree root with graphene oxide decorated surface (DRGO). As was evident from Fig. 3a, the ratio of carbon and oxygen changed after graphene oxide loading. The peak corresponding to the oxidized sp^3 domains (C═O/O-C-O) for DRGO was slightly increased compared with DR, indicating the successful deposition of graphene oxide (Fig. 3b and c). XRD pattern of the fabricated DRGO showed two typical diffraction peaks of graphene oxide at 10.8 ° and 34.6 °, respectively, further confirming the formation of graphene oxide layer (Fig. 3d). We also tested the structure-stability of the graphene oxide decorated tree root by immersing in acidic (pH=1) and base (pH=14) solution for 12 h and further ultrasonication in pure water for

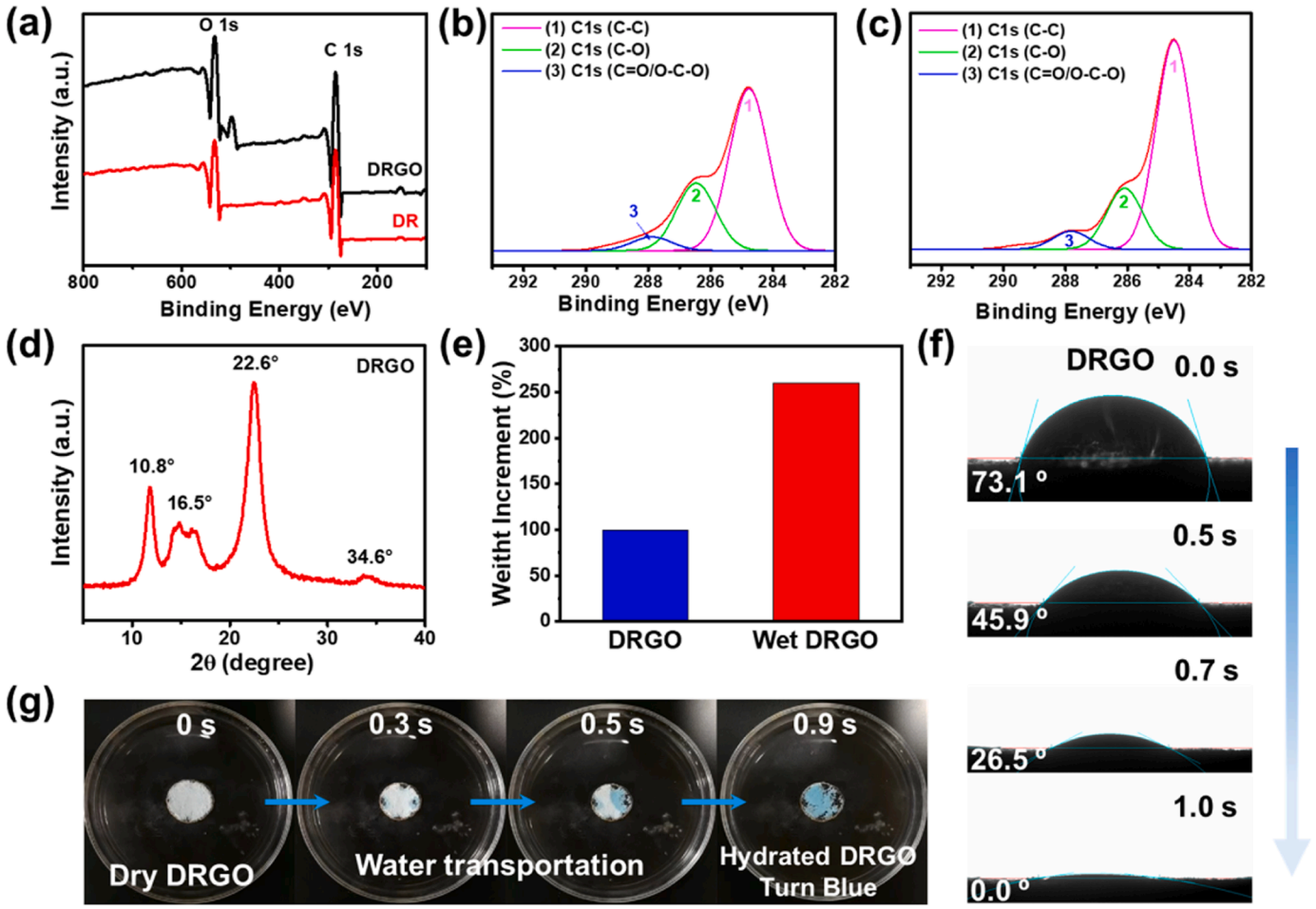

Fig. 3. XPS survey scan (a) and high-resolution C 1 s spectra of the DR (b) and DRGO (c). (d) XRD pattern of the DR and DRGO. (e) The weight change of the DRGO before and after wetting. The thickness of the DRGO in this experiment was 3 mm. (f) Change of contact angle with time. (g) Digital images showing that the color of the DRGO turns from white to blue while quickly absorbing water (surface covered with anhydrous copper sulfate as indicator).

30 min. No changes were observed for the evaporator and the used solutions before and after above treatments, indicating a high structure stability of the loading graphene oxide on the tree root surface to the various working environment (Fig. S4). The weight changes of the dry and wet DRGO were evaluated after being immersed in water. The weight of the wet DRGO increased form 100% to ≈ 260%, indicating an excellent spontaneous water absorption capability, which ensured the continuous water supply during water evaporation loss at the top surface of the desalination device (Fig. 3e). Moreover, due to its inherent porous microstructure and low density (Fig. S6), the fabricated tree root-based solar evaporator still retained internal pores and could float on the water surface.

The multi-level channels of tree root undertake bottom-to-top water transported to continuously supply the water loss due to the stream evaporation on the top solar absorber layer. The natural tree root contained large number of hydrophobic components, such as its inherent lignin, exhibiting low water permeability which could limit water transportation. The initial contact angle of tree root surface (117.6°) showed hydrophobic property, making the water droplet hard to be absorbed completely after 50 s (Fig. S5). However, after partly delignification of natural tree root, the water droplet can rapidly penetrate into the lower substrate within 1 s after it touched the surface (Fig. 3f), thus achieving excellent water transportation capability by the enhanced capillary penetration. As shown in Fig. 3g, once the bottom surface of the solar desalination device contacted with water, the top layer was thoroughly wetted within 0.9 s, demonstrating the super rapid capillary water transport through the inner highly hydrophilic multi-level channels. The excellent water transportation capacity was also an essential factor for preventing salt accumulation on the evaporator's surface and the channel blockage by offering adequate water supply and automatic rapid salt exchange. Therefore, a facile bilayered interfacial evaporation device composed of black graphene oxide layer and superhydrophilic tree root substrate is designed.

3.2. Photothermal conversion property of DRGO

The decorated graphene oxide on the surface of tree root continuously absorbed sunlight and converted it into heat (Fig. 4a). The light absorbability and photothermal conversion ability of absorber layer played a vital role in evaporation efficiency of solar desalination device. The UV–vis–NIR spectroscopy demonstrated that the graphene decorated tree root evaporator exhibited excellent light absorption (Fig. 4b), which was much higher than that of the delignificated tree root. This was mainly attributed to the broad absorption spectrum of graphene oxide and the abundant protrusion microstructures on the evaporator surface which was favorable for enhancing the light absorption and reducing reflection. The outstanding solar absorption ability was beneficial for promoting the efficiency of light-to-thermal conversion.

The temperature variation of graphene oxide decorated tree root in the wet state was traced by an infrared radiation camera under one sun illumination (Fig. 4c and d). The temperature of the top surface increased rapidly to 35.3 °C from room temperature after 10 min and gradually reached the highest temperature of 36.8 °C after 80 min. In contrast, the highest temperature of the delignificated tree root without graphene oxide modification was only 32 °C. The results of thermal conductivity showed that the delignificated tree root presented relatively low thermal conductivity of 0.21 W m^{-1} K^{-1} and 0.20 W m^{-1} K^{-1} in the crossplane direction (R) and the growth direction (L), respectively (Fig. 4e), which could limit heat diffusion of the solar evaporator. Therefore, the excellent photothermal conversion property can be attributed to two reasons. Firstly, the rough bumpy surface microstructure of evaporator absorber layer achieved high light absorbance, efficiently harvesting sunlight over a broad range of spectrum. The second was excellent thermal localization management due to the low thermal conductivity of the bottom tree root substrate of the solar evaporator.

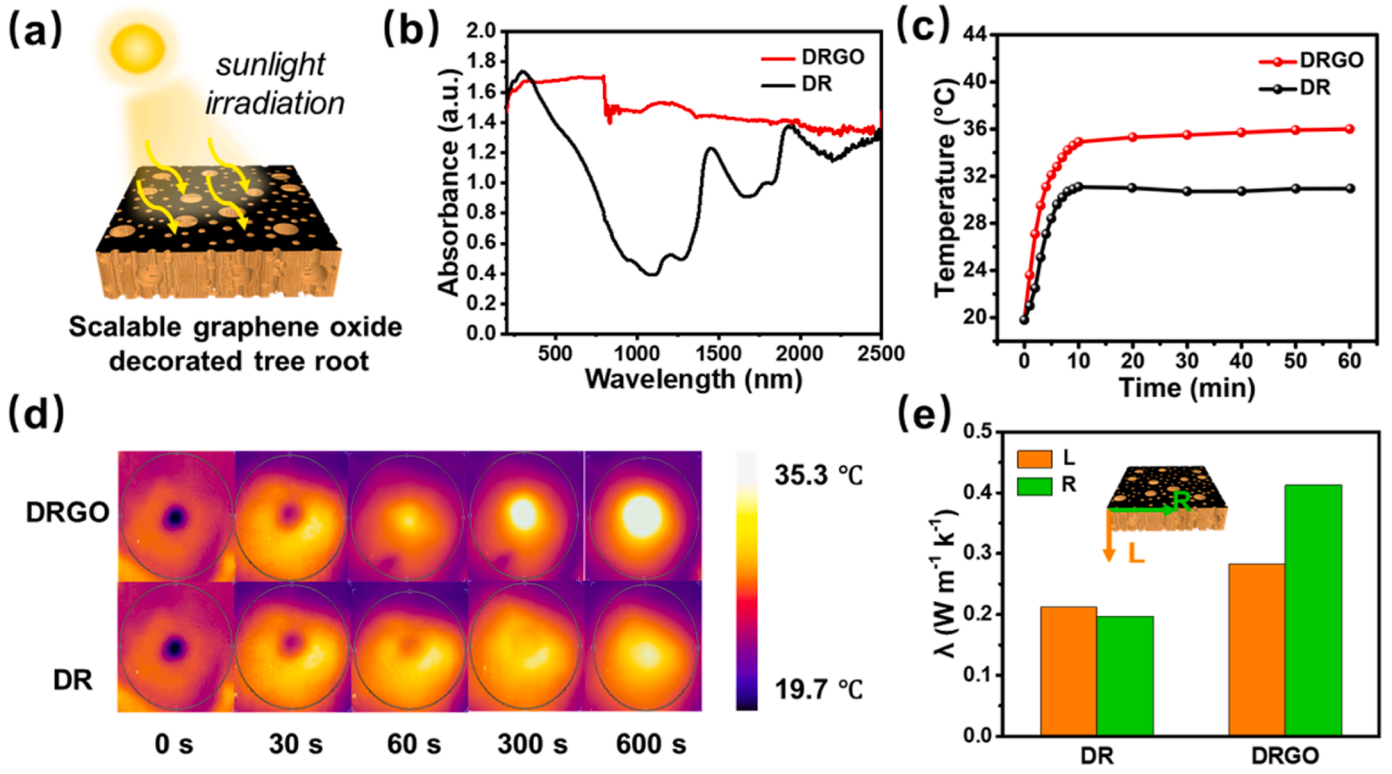

Fig. 4. (a) Schematic showing the sunlight absorption of the scalable graphene oxide decorated tree root. (b) Absorbance comparison between DR and DRGO. Time-dependent average temperature (c) and IR images (d) showing in situ temperature change of DRGO under 1 sun irradiation. (e) Thermal conductivity of the DR and DRGO.

3.3. Desalination performance of DRGO

Owing to the excellent water transport capability and photothermal conversion property, the bilayer designed solar evaporator can be expected to have extraordinary performance for solar desalination. The solar steam efficiency was calculated by subtracting the mass loss of pure water evaporation to ensure the reliability of the experimental values. Fig. 5a showed that the mass change (water evaporation rate) for the fabricated graphene oxide decorated tree root (DRGO) is significantly faster than that of the undecorated tree root (DR). The evaporation rates of DRGO and DR increased rapidly in the initial 5 min and reached a plateau after 10 min (Fig. 5b). The overall trend of evaporation rate fitted quite well with the heating process of the top absorber layer, indicating the rapid response performance for the fabricated solar evaporator. The output stable evaporation rate of DRGO reached 1.60 kg m^{-2} h^{-1}, which was significantly higher than that of control sample (Fig. 5c). More impressively, the calculated evaporation efficiency reached an astonishing 96.5%, which was the almost highest record among the various wood-based desalination devices (Table 1). The excellent performance of the graphene oxide decorated tree root could be ascribed to its outstanding solar-thermal conversion ability by the coated rough absorber surface which ensured an excellent broadband light absorption. Furthermore, the hydrophilic tree root substrate set the evaporator a continuous water supply capability through the abundant multilevel channels.

3.4. Anti-salt-accumulation performance of the DRGO

Note that it is difficult to remain long-term stable desalination by conventional solar evaporators due to the continuous salt accumulation on the absorber surface. Here, the stability of our fabricated tree root-based evaporator was tested. The stable solar evaporation performance was achieved during the 72 h continuously working in 3.5 wt% NaCl solution under 1 sun illumination (Fig. 6a and b). We also carefully evaluated the long-term stability of our evaporator under different brine concentration varying from 3.5% to 21%. Results revealed the excellent adaptability and anti-salt-accumulation property of our fabricated evaporator (Fig. 6c). As shown in Fig. 6d, the graphene oxide decorated tree root evaporator (DRGO) exhibited superior salt-rejecting performance even in 21 wt% NaCl solution for 72 h, while the absorber surface of the wood-based evaporator was covered by numerous white salt crystals. The white salt layer would reduce the light absorption and decrease the evaporation rate and stability of desalination process. These results indicated the key roles of the large channels of tree root for stable solar desalination, thus exhibiting the excellent anti-salt-accumulation performance. With the interconnected multilevel channel microstructures, the concentrated brine in the narrow channels caused by continuous evaporation can be rapidly diluted into the large channels with low concentration in real-time (Fig. 6e). Natural large channels in tree root performed the same function as artificial drilling of wood for the salt-rejecting solar desalination process (Kuang et al., 2019; Sharshir et al., 2022). For the wood trunk-based evaporator, the brine concentration of the micron-scale vertically channels maintains at the same level, the concentration difference driving force was not enough to promote extensive salt exchange. Therefore, compared to traditional designed evaporator, our results illustrated that the tree root-based evaporator demonstrated significantly improved efficiency and anti-salt-accumulation property, giving it great potential for scalable steam-generation applications.

Table 1
Performance comparison of current reported wood based solar-steam-generation devices.

Wood species	Photothermal materials or methods	Efficiencies (%)	Evaporation rates (kg m^{-2} h^{-1})	Ref
Poplar	Carbonized wood	86.7 (10 suns)	12.1 (10 suns)	(Jia et al., 2017)
Basswood	Graphite	80	1.15	(Li et al., 2018)
Balsa wood	Delignification (Fe_3O_4)	73	1.3	(Song et al., 2021)
Pine wood	Carbon black	93.4 (3.5 suns)	3.38 (3.5 suns)	(Duan et al., 2022)
Basswood	Catechin–Fe^{3+}	54	0.92	(Gao et al., 2020)
Paulownia wood	Ti_3C_2 nanosheets	96	1.465	(Ma et al., 2020)
Tree root	Graphene oxide	96.5	1.6	This work

4. Conclusions

We demonstrated that the bilayer designed evaporator (e.g. tree root-based evaporator) with intrinsic microstructure could achieve a high-efficient and long-term brine desalination. The unique multilevel longitudinal channel structure played a vital role in effectively overcoming the salt-accumulation related issues. Specifically, ultra-high-speed water transport capability and the concentration difference driving force between the multistage channels in the hydrophilic tree root evaporator led to rapid multi-directional salt exchange to prevent salt accumulation on the top evaporation surface, thus ensuring efficient and continuous solar desalination. Together with graphene oxide decorated absorber surface, a rapid evaporation rate with excellent long-term stability was achieved even in a high-salinity brine (21 wt%). In contrast, during desalination process, the top surface of the wood trunk-

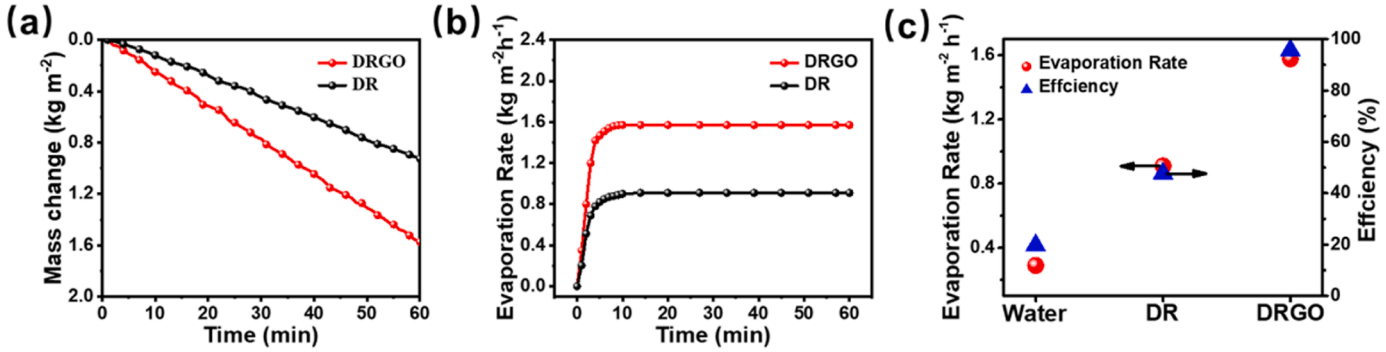

Fig. 5. (a) Mass change of water desalinated by the DR and DRGO over time. (b) Evaporation rate of the DR and DRGO. (c) Comparison of evaporation performance of 3.5%wt saline water, DR, DRGO. (under 1 sun irradiation in the desalination of 3.5% salt solution).

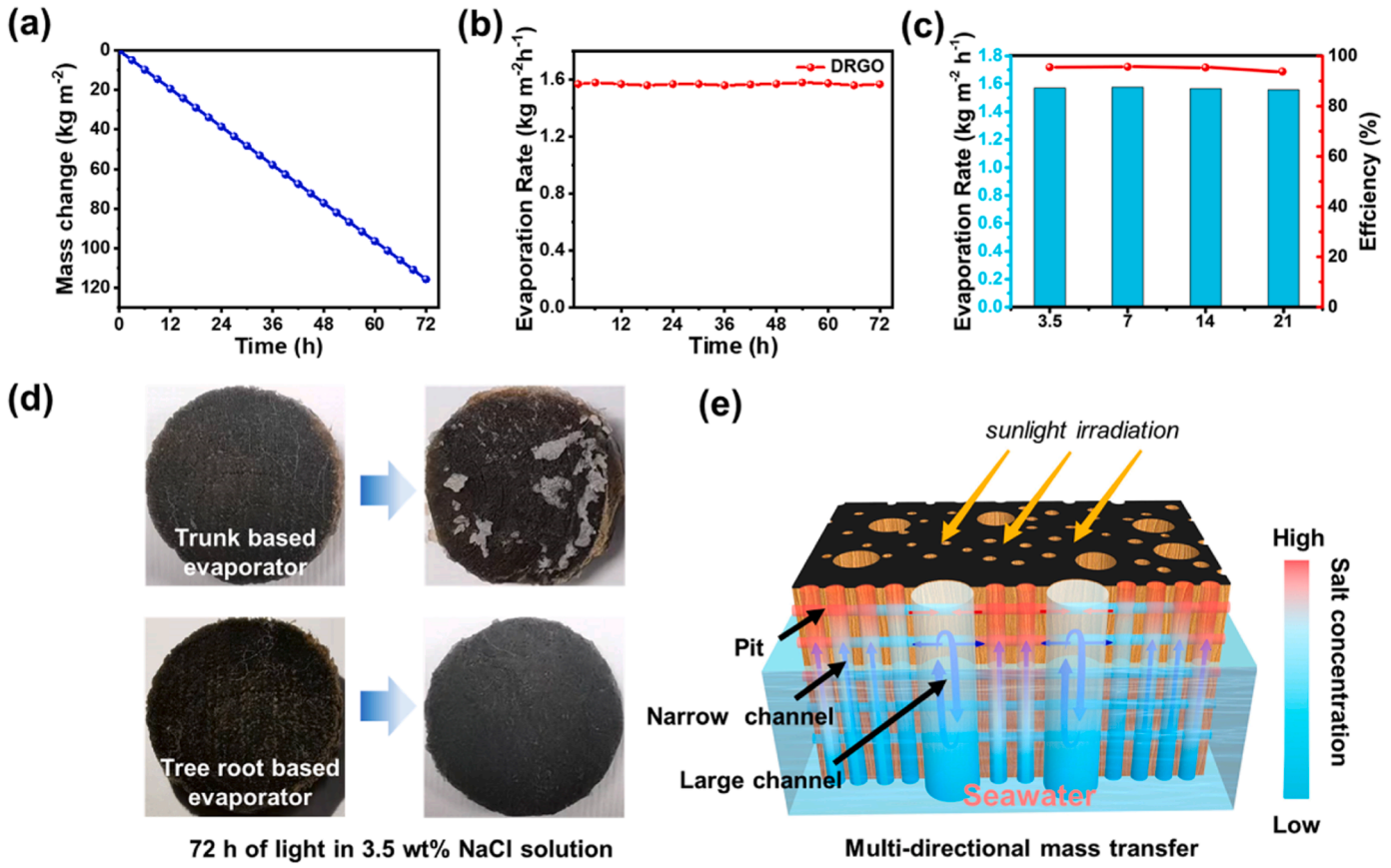

Fig. 6. 72 h continuous-desalination performance on the mass change (a) and evaporation rate (b) of DRGO. (c) The influence of salt concentration on the desalination performance of DRGO. (d) Comparation of salt-rejecting performance of wood trunk and tree root -based desalination device. (e) The anti-salt-accumulation mechanism of the designed tree root based evaporator.

based evaporator was covered by numerous white salt crystals which severely reduced the light absorption and decreased the evaporation rate and stability of the solar evaporator. Benefiting from the renewable, widespread, high efficiency and anti-salt-accumulation capability, our bilayered tree root-based evaporator possesses a promising desalination strategy for sustainable and scalable clean water production.

CRediT authorship contribution statement

Yongzheng Li: Methodology, Validation, Writing – original draft. **Xiaodi Wang**: Resources, Formal analysis, Validation, Writing – original draft. **Ruijie Wu:** Investigation, Validation. **Jinli Qin:** Methodology, Formal analysis, Validation. **Yingjuan Fu:** Writing – review & editing, Supervision, Funding acquisition. **Menghua Qin:** Writing – review & editing, Supervision. **Yongchao Zhang:** Conceptualization, Supervision, Funding acquisition, Writing – review & editing. **Chunlin Xu:** Conceptualization, Supervision, Writing – review & editing.

Declaration of Competing Interest

The authors declare that they have no known competing financial interests or personal relationships that could have appeared to influence the work reported in this paper.

Data Availability

Data will be made available on request.

Acknowledgements

The project was supported by the National Natural Science Foundation of China (No. 32001269 and 32271821), China Postdoctoral Science Foundation (No. 2021M701287), QUTPY Project (No. 2022PY023) the QUTJBZ Program (No. 2022JBZ01–05) and the Jinan Independently Cultivate Innovative Team (202228076).

Appendix A. Supporting information

Supplementary data associated with this article can be found in the online version at doi:10.1016/j.indcrop.2023.117649.

References

Al-Douri, Y., Fayadh, M.A., 2016. Solar energy status in Iraq: abundant or not—steps forward. J. Renew. Sustain. Energy 8 (2), 025905.
Bian, Y., Tang, K., Tian, L.Y., Zhao, L.J., Zhu, S.M., Lu, H., Yang, Y., Ye, J.D., Gu, S.L., 2021. Sustainable solar evaporation while salt accumulation. ACS Appl. Mater. Inter. 13 (4), 4935–4942.
Cao, S., Rathi, P., Wu, X., Ghim, D., Jun, Y.S., Singamaneni, S., 2021. Cellulose nanomaterials in interfacial evaporators for desalination: a “natural” choice. Adv. Mater. 33 (28), 2000922.
Chen, C.J., Li, Y.J., Song, J.W., Yang, Z., Kuang, Y., Hitz, E., Jia, C., Gong, A., Jiang, F., Zhu, J.Y., Yang, B., Xie, J., Hu, L.B., 2017. Highly flexible and efficient solar steam generation device. Adv. Mater. 29 (30), 1701756.
Chen, C.J., Kuang, Y.D., Hu, L.B., 2019. Challenges and opportunities for solar evaporation. Joule 3 (3), 683–718.
Dengyu, L., Xuejiao, Z., Siyu, Z., Dongsheng, W., Zhenyu, W., Ying, L., Xuefeng, Y., Qing, Z., Baoshan, X., 2020. A flexible and salt-rejecting electrospun film-based solar evaporator for economic, stable and efficient solar desalination and wastewater treatment. Chemosphere 267.
Djellabi, R., Noureen, L., Dao, V., Meroni, D., Falletta, E., Dionysiou, D.D.D., Bianchi, C. L., 2022. Recent advances and challenges of emerging solar-driven steam and the contribution of photocatalytic effect. Chem. Eng. J. 431, 134024.

Duan, H., Wang, Y., Yan, Y., Ling, T., 2022. Evaporation performance of wood-based evaporator for solar interfacial vapor generation. Energy Technol. 10 (4), 2101020.
Duan, Y., Weng, M., Zhang, W., Qian, Y., Luo, Z., Chen, L., 2021. Multi-functional carbon nanotube paper for solar water evaporation combined with electricity generation and storage. Energ. Convers. Manag. 241, 114306.
Fujun, T., Yuliang, Z., Kuan, Y., Shengjia, C., Xueting, C., Yanhua, L., Dongsheng, W., Runhua, F., Lihua, D., Yansheng, Y., Xiaobo, C., 2018. A plasmonic interfacial evaporator for high-efficiency solar vapor generation. Sustain. Energ. Fuels 2 (12), 2762–2769.
Gao, H., Yang, M.M., Dang, B., Luo, X.F., Liu, S.X., Li, S.J., Chen, Z.J., Li, J., 2020. Natural phenolic compound-iron complexes: sustainable solar absorbers for wood-based solar steam generation devices. RSC Adv. 10 (2), 1152–1158.
Han, X.M., Besteiro, L.V., Koh, C.S.L., Lee, H.K., Phang, I.Y., Phan-Quang, G.C., Ng, J.Y., Sim, H.Y.F., Lay, C.L., Govorov, A., Ling, X.Y., 2021. Intensifying heat using MOF-isolated graphene for solar-driven seawater desalination at 98% solar-to-thermal efficiency. Adv. Funct. Mater. 31 (13), 2008904.
He, C., Liu, Z., Wu, J., Pan, X., Fang, Z., Li, J., Bryan, B.A., 2021. Future global urban water scarcity and potential solutions. Nat. Commun. 12 (1), 4667.
He, S., Chen, C., Kuang, Y., Mi, R., Liu, Y., Pei, Y., Kong, W., Gan, W., Xie, H., Hitz, E., 2019. Nature-inspired salt resistant bimodal porous solar evaporator for efficient and stable water desalination. Energ. Environ. Sci. 12 (5), 1558–1567.
Jia, C., Li, Y., Yang, Z., Chen, G., Yao, Y., Jiang, F., Kuang, Y., Pastel, G., Xie, H., Yang, B., 2017. Rich mesostructures derived from natural woods for solar steam generation. Joule 1 (3), 588–599.
Jingjing, X., Jintao, T., Ye, L., Yutong, G., Lanjian, Z., Dafeng, Z., Ruomeng, D., Bo, S., Yu, Z., Bin, D., 2020. A high-efficiency ammonia-responsive solar evaporator. Nanoscale 12 (17), 9680–9687.
Kuang, Y., Chen, C., He, S., Hitz, E.M., Wang, Y., Gan, W., Mi, R., Hu, L., 2019. A high-performance self-regenerating solar evaporator for continuous water desalination. Adv. Mater. 31 (23), 1900498.
Kumar, R., Raizada, P., Verma, N., Hosseini-Bandegharaei, A., Thakur, V.K., Le, Q.V., Nguyen, V.-H., Selvasembian, R., Singh, P., 2021. Recent advances on water disinfection using bismuth based modified photocatalysts: strategies and challenges. J. Clean. Prod. 297, 126617.
Kummu, M., Guillaume, J.H.A., de Moel, H., Eisner, S., Flörke, M., Porkka, M., Siebert, S., Veldkamp, T.I.E., Ward, P.J., 2016. The world's road to water scarcity: shortage and stress in the 20th century and pathways towards sustainability. Sci. Rep. 6 (1), 38495.
Li, J., Chen, S., Li, X., Zhang, J., Nawaz, H., Xu, Y., Kong, F., Xu, F., 2023. Anisotropic cellulose nanofibril aerogels fabricated by directional stabilization and ambient drying for efficient solar evaporation. Chem. Eng. J. 453 (2), 139844.
Li, T., Liu, H., Zhao, X., Chen, G., Dai, J., Pastel, G., Jia, C., Chen, C., Hitz, E., Siddhartha, D., 2018. Scalable and highly efficient mesoporous wood-based solar steam generation device: localized heat, rapid water transport. Adv. Funct. Mater. 28 (16), 1707134.
Ma, N., Fu, Q., Hong, Y., Hao, X., Wang, X., Ju, J., Sun, J., 2020. Processing natural wood into an efficient and durable solar steam generation device. ACS Appl. Mater. Interfaces 12 (15), 18165–18173.
Mekonnen, M.M., Hoekstra, A., 2016. Four billion people facing severe water scarcity. Sci. Adv. 2 (2), e1500323.
Peng, Y.Y., Zhao, W.W., Ni, F., Yu, W.J., Liu, X.Q., 2021. Forest-like laser-induced graphene film with ultrahigh solar energy utilization efficiency. ACS Nano 15 (12), 19490–19502.
Rana, A.K., Gupta, V.K., Saini, A.K., Voicu, S.I., Abdellattifaand, M.H., Thakur, V.K., 2021. Water desalination using nanocelluloses/cellulose derivatives based membranes for sustainable future. Desalination 520, 115359.
Sharshir, S.W., Kandeal, A.W., Ellakany, Y.M., Maher, I., Khalil, A., Swidan, A., Abdelaziz, G.B., Koheil, H., Rashad, M., 2022. Improving the performance of tubular solar still integrated with drilled carbonized wood and carbon black thin film evaporation. Sol. Energy 233, 504–514.
Song, L., Zhang, X.-F., Wang, Z., Zheng, T., Yao, J., 2021. Fe3O4/polyvinyl alcohol decorated delignified wood evaporator for continuous solar steam generation. Desalination 507, 115024.
Storer, D.P., Phelps, J.L., Wu, X., Owens, G., Khan, N.I., Xu, H.L., 2020. Graphene and rice-straw-fiber-based 3D photothermal aerogels for highly efficient solar evaporation. ACS Appl. Mater. Inter. 12 (13), 15279–15287.
Weixin, G., Youhong, G., Guihua, Y., 2021. Carbon materials for solar water evaporation and desalination. Small 17 (48), 2007176.
Xue, G., Liu, K., Chen, Q., Yang, P., Li, J., Ding, T., Duan, J., Qi, B., Zhou, J., 2017. Robust and low-cost flame-treated wood for high-performance solar steam generation. ACS Appl. Mater. Inter. 9 (17), 15052–15057.
Zang, L.L., Finnerty, C., Zheng, S.X., Conway, K., Sun, L.G., Ma, J., Mi, B.X., 2021. Interfacial solar vapor generation for desalination and brine treatment: Evaluating current strategies of solving scaling. Water Res. 198, 117135.
Zheng, J., Wang, W., Yu, D., Wang, W., 2023. Carbon nanotubes@polydopamine/nickel foam with a wavy shape applied for efficient solar-driven seawater desalination. Desalination 567, 116961.
Zhu, M., Li, Y., Chen, F., Zhu, X., Dai, J., Li, Y., Yang, Z., Yan, X., Song, J., Wang, Y., 2018. Plasmonic wood for high-efficiency solar steam generation. Adv. Energ. Mater. 8 (4), 1701028.